

# Three-dimensional sub-100 nm resolution fluorescence microscopy of thick samples

Manuel F Juetten<sup>1,2</sup>, Travis J Gould<sup>3,4</sup>,  
Mark D Lessard<sup>1</sup>, Michael J Mlodzianowski<sup>1</sup>,  
Bhupendra S Nagpure<sup>1,3</sup>, Brian T Bennett<sup>5</sup>,  
Samuel T Hess<sup>3,4</sup> & Joerg Bewersdorff<sup>1</sup>

**Imaging volumes as thick as whole cells at three-dimensional (3D) super-resolution is required to reveal unknown features of cellular organization. We report a light microscope that generates images with translationally invariant  $30 \times 30 \times 75$  nm resolution over a depth of several micrometers. This method, named biplane (BP) FPALM, combines a double-plane detection scheme with fluorescence photoactivation localization microscopy (FPALM) enabling 3D sub-diffraction resolution without compromising speed or sensitivity.**

In contrast to techniques such as electron, X-ray or atomic force microscopy, light microscopy is capable of providing 3D images of cells several micrometers thick. This and other unique abilities have made it the most widely used biological imaging technique today, despite the higher spatial resolution of alternative methods. Until roughly a decade ago, resolution in far-field light microscopy was limited to  $\sim 200$ – $250$  nm within the focal plane, concealing details of sub-cellular structures and constraining biological applications. Today, stimulated emission depletion (STED) microscopy, and other members of the reversible saturable optical fluorescence transitions (RESOLFT) family, are able to overcome the diffraction barrier and achieve biological imaging at resolutions below  $\sim 20$  nm using the seminal concept of point-spread function (PSF) engineering through optically saturable transitions of the (fluorescent) probe molecules<sup>1</sup>.

Recently, an emerging group of localization-based techniques called FPALM<sup>2</sup>, PALM<sup>3</sup>, stochastic optical reconstruction microscopy (STORM)<sup>4</sup> and PALM with independently running acquisition (PALMIRA)<sup>5,6</sup> has permitted comparable lateral resolution. Although they use similar optical switching mechanisms, techniques in this latter group circumvent the diffraction limit by basing

resolution improvement on the precise localization of spatially well-separated fluorescent molecules as used in particle-tracking techniques<sup>7</sup>.

To resolve complex nanoscale structures by localization-based methods, the sample is labeled with photoactivatable or photo-switchable fluorescent probes. Activation of only a sparse subset of molecules at a time allows their separate localization. By repeated bleaching or deactivation of the active molecules in concert with activation of other inactive probe molecules, a large fraction of the whole probe ensemble can be localized over time to produce a two-dimensional sub-diffraction image of the labeled structure.

However, to investigate complex cellular structures 3D imaging is required. The best 3D resolution in light microscopy until lately had been  $\sim 100$  nm axially at conventional lateral resolution using 4Pi microscopy<sup>8</sup>. Recent reports demonstrated 3D STED microscopy exceeding conventional resolution two to fourfold with 139-nm lateral ( $x,y$ ) and 170-nm axial ( $z$ ) resolution<sup>9</sup>, and 3D STORM of thin optical sections ( $< 600$  nm) with sub-100 nm 3D resolution under reducing (low oxygen) conditions<sup>10</sup>.

We now show 3D imaging of 'thick' samples over a depth of several micrometers at a resolution of  $\sim 30$  nm laterally and 75 nm axially achieved by BP FPALM. The microscope design is based on a conventional FPALM design<sup>2</sup> with a modified detection path that allows simultaneous detection from two axially separated object planes (Fig. 1a). Illumination for readout and activation is provided by lasers operating typically at 496 nm and 405 nm, respectively. Both lasers are coupled into a conventional microscope stand equipped with a  $63\times 1.2$  numerical aperture (NA) water immersion lens. A high-sensitivity electron-multiplying charge-coupled device (EM-CCD) camera collects the fluorescence (Supplementary Methods online). In the biplane detection scheme, a 50:50 beam splitter cube divides the focused light in front of the camera into a transmitted (shorter) and a reflected (longer) path, which is redirected toward the camera. The transmitted and reflected beams form images on different regions of the detector representing object planes  $\sim 350$  nm further away and closer to the objective than the original object plane, respectively.

The signal from the two recorded regions of interest can, therefore, be combined into a 3D raw data stack consisting of two planes. Data analysis is a generalization of standard FPALM methods to three dimensions (Supplementary Methods). Instead of a Gaussian, we fit an experimentally obtained 3D PSF to each dataset consisting of the pixels around each detected probe molecule, thereby determining its  $x$ ,  $y$  and  $z$  coordinates. The PSF is determined independently by imaging a small fluorescent bead as

<sup>1</sup>Institute for Molecular Biophysics, The Jackson Laboratory, 600 Main Street, Bar Harbor, Maine 04609, USA. <sup>2</sup>Department of Biophysical Chemistry, University of Heidelberg, and Department of New Materials and Biosystems, Max Planck Institute for Metals Research, Heisenbergstr. 3, 70569 Stuttgart, Germany. <sup>3</sup>Department of Physics and Astronomy, University of Maine, 120 Bennett Hall, Orono, Maine 04469, USA. <sup>4</sup>Institute for Molecular Biophysics, University of Maine, 5737 Jenness Hall, Orono, Maine 04469, USA. <sup>5</sup>Active Motif, Inc., 1914 Palomar Oaks Way, Carlsbad, California 92008, USA. Correspondence should be addressed to J.B. (joerg.bewersdorff@jax.org).

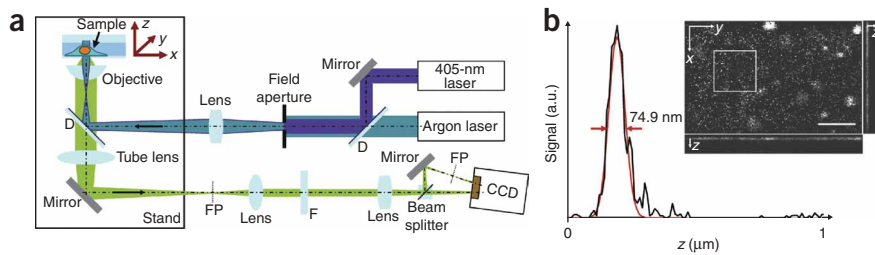
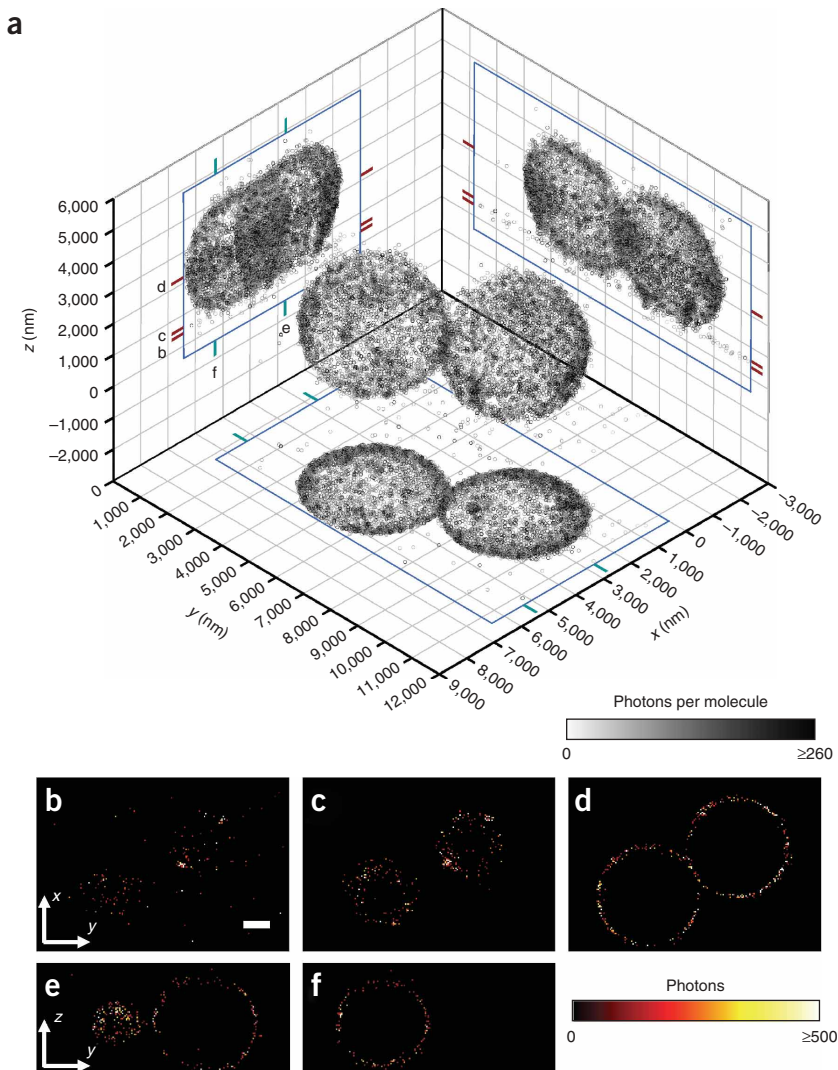


**Figure 1** | BP FPALM setup and axial resolution. **(a)** Lasers are coupled into a conventional microscope for widefield activation and excitation of photoactivatable fluorescent molecules. Collected fluorescence is divided by a 50:50 beam splitter, creating two separate image planes on the same CCD camera. D, dichroic beamsplitter; FP, focal plane; F, bandpass filter. **(b)** Histogram of localized caged fluorescein-labeled antibodies on a coverslip as a function of  $z$ -axis position. The inset shows summed projections of the obtained dataset in three different directions. The white box marks the region of the original 3D dataset used to generate the shown  $z$  profile. Black line, raw data; red line, Gaussian fit. Scale bar,  $2\ \mu\text{m}$ .

a function of the  $z$ -dimension position of the sample relative to the objective (**Supplementary Methods**).

Use of two detection planes for  $z$  position determination is generally sufficient for particle localization under the constraints that (i) a sparse distribution of particles is analyzed (no overlapping signal within the size of one PSF) and (ii) the axial position of the particle is close to one of the detection planes or lies between them. To evaluate the range and accuracy of the  $z$  localization, we imaged 40 nm diameter fluorescent beads (FluoSpheres; Invitrogen) on a coverslip for 1,000 frames. The piezo-driven sample stage was moved by one 100-nm  $z$ -step every 100 frames. Localization analysis of the BP FPALM images reproduced that  $z$ -direction movement very accurately with a standard deviation in axial localization of  $\sim 6$ – $10$  nm axial localization accuracy (**Supplementary Fig. 1** online). The beads could be localized over a range of 800 nm, exceeding the distance between the two detection planes (in this case 500 nm) by more than 50%.

**Figure 2** | 3D BP FPALM of  $4\ \mu\text{m}$  diameter beads labeled with caged fluorescein. **(a)** Localized molecules are denoted by open circles in the 3D representation as well as in projections along the  $x$ ,  $y$  and  $z$  axes. The color of the circles indicates the number of photons detected from each molecule as shown by the gray scale color bar. The blue boxes in the projections show the reconstructed 3D volume defined by the regions of interest in  $x$  and  $y$  dimensions and by the scan range in the  $z$  dimension. **(b–f)** Representative  $y$ - $x$  and  $y$ - $z$  sections through the reconstructed 3D volume showing all localized molecules within  $\pm 50$  nm of each plane (localized molecules binned into pixels of  $25 \times 25\ \text{nm}^2$  size). The pixel color denotes the sum of detected photons from the localized molecules falling in each pixel as shown in the color bar below. The position and orientation of the sections is indicated in **a**. Scale bar,  $1\ \mu\text{m}$ .



The detection of multiple focal planes in biological samples has independently been reported for particle tracking in related experimental geometries<sup>11–13</sup>. For localization-based super-resolution microscopy, the simultaneous detection of two planes has two important advantages. First, the imaging process is sped up by making axial scanning completely unnecessary for volumes less than  $\sim 1\ \mu\text{m}$  thick. More importantly, it eliminates localization artifacts present in scanning-based systems caused by the abrupt blinking and bleaching common to single molecules.

To prove the feasibility of BP FPALM with single molecules and to measure the axial resolution, we imaged caged fluorescein (Invitrogen) bound to antibodies on a coverslip and embedded in 87% glycerol (**Fig. 1b**). To allow a direct comparison with conventional microscopy, the localized molecules were binned according to their positions in voxels of  $50 \times 50 \times 10\ \text{nm}$  ( $x \times y \times z$ ) in size, forming a 3D data stack. Voxel intensities

cein (Invitrogen) bound to antibodies on a coverslip and embedded in 87% glycerol (**Fig. 1b**). To allow a direct comparison with conventional microscopy, the localized molecules were binned according to their positions in voxels of  $50 \times 50 \times 10\ \text{nm}$  ( $x \times y \times z$ ) in size, forming a 3D data stack. Voxel intensities

were assigned by adding the detected photon numbers of all molecules in that voxel. From the histogram of localized molecules as a function of  $z$  position (Fig. 1b), we measured a full width at half-maximum (FWHM) of 75 nm. The true  $z$ -resolution of BP FPALM is potentially even better considering that this histogram may be broadened by a slightly curved, rough or tilted coverslip surface. The obtained value is about tenfold below the axial FWHM of our measured PSF, which represents the axial resolution of conventional diffraction-limited microscopy. As localization-based resolution is proportional to the diffraction-limited PSF size and the axial FWHM of a widefield 1.2 NA PSF is  $\sim 250\%$  larger than the lateral FWHM, our measured  $z$ -direction localization precision is consistent with the  $x$  and  $y$  resolution of 20–40 nm previously obtained in FPALM<sup>2,14</sup> and PALM<sup>3</sup>.

Notably, as we confirmed experimentally (Supplementary Fig. 2 online), the biplane detection scheme of BP FPALM results in lateral and axial resolution values that are virtually independent of the localization depth range of  $\sim 1 \mu\text{m}$ . In contrast, in astigmatism-based axial localization methods as used by others<sup>10</sup>, which analyze the ellipticity of the diffraction-limited image, the  $x$  and  $y$  localization accuracies are not translationally invariant and change with the axial probe position with their ratio rising from  $\sim 0.5$  to  $\sim 2$  over the same axial  $1 \mu\text{m}$  detection range. To achieve more spatially homogeneous resolution, the axial localization range has to be reduced to about half that range<sup>10</sup>. Furthermore the dipole orientation of fluorescent probes can lead to strong ellipticity of the detected fluorescent spot<sup>7</sup>. This intermingles the probe orientation with the determined axial probe position and can cause strong axial localization artifacts in astigmatism-based localization methods. In contrast, BP FPALM's axial localization mechanism is far less sensitive to ellipticity. In principle, BP FPALM data can be analyzed in parallel for axial position and for ellipticity to determine the probe orientation.

The wide axial localization range of BP FPALM makes this technique highly suitable for imaging of thick volumes, by combining BP FPALM data recorded at different sample stage positions. To demonstrate the distortion-free 3D imaging capabilities of samples thicker than the axial localization range of  $\sim 1 \mu\text{m}$  of our BP FPALM microscope, we imaged  $4 \mu\text{m}$  diameter spherical beads surface-labeled with caged fluorescein. To image the beads over their complete thickness, we recorded BP FPALM data at different  $z$  positions of the sample stage and combined the localization results corrected for the  $z$ -position offset of the stage (Supplementary Methods). The localized positions of 8,934 particles reproduced the spherical surfaces of two adjacent beads ( $\sim 100$  particles/ $\mu\text{m}^2$  surface density) without artifacts over the complete depth (Fig. 2). This confirms that BP FPALM is capable of distortion-free imaging over the complete depth of large 3D objects.

To our knowledge, these are the first optical images with well-below 100 nm resolution in all three dimensions of a sample far exceeding the size of a PSF in all directions (Fig. 2). The resolvable volume of approximately  $30 \times 30 \times 75 \text{ nm}$  is  $\sim 500$ -fold below the diffraction-limited observation volume. Furthermore, BP FPALM is capable of 3D imaging of volumes  $\leq 1 \mu\text{m}$  thickness without scanning (Supplementary Fig. 3 online).

Our compact, cost-efficient, robust design using only one camera is straightforward to implement and avoids synchronization problems between separate cameras. With our setup, we were able to image 100 frames per second with a field of view of 10–20  $\mu\text{m}$  in length and  $2 \times 2$  binning. Combined with the fact that we have minimal loss of fluorescence detection efficiency, this setup expands conventional FPALM to 3D imaging without major drawbacks.

The existing BP FPALM technology is fully compatible with live-cell imaging as it does not require reducing conditions as in STORM. Volumes  $1 \mu\text{m}$  thick can be imaged at the same speed as 2D FPALM, which, with presently available camera technology, can be as low as several seconds. BP FPALM can also be easily expanded to multicolor imaging. To minimize activation of out-of-focus molecules, BP FPALM can be combined with a scanning two-photon excitation laser beam. Two-photon excitation-mediated activation is limited to diffraction-limited planes<sup>6,15</sup> of  $\sim 800 \text{ nm}$  thickness, a thickness that is fully compatible with the axial detection range of BP FPALM. BP FPALM therefore has the potential to image specimens such as tissue sections many micrometers thick.

Moreover, BP FPALM can be readily implemented in practically every existing FPALM, PALM, PALMIRA or STORM instrument. BP FPALM featuring a 100–1,000-fold smaller resolvable volume than obtainable by conventional 3D microscopy, therefore, provides the means to investigate a large variety of biological 3D structures at resolution levels previously far out of reach.

Note: Supplementary information is available on the Nature Methods website.

#### ACKNOWLEDGMENTS

We thank L. Rocco Carpenter for purification and antibody-conjugation of the caged fluorescein, Th. Tripp for machining services, E. Burns and B. Knowles for valuable comments on the manuscript and J. Spatz for support. This work was supported by the US National Institute of Allergy and Infectious Diseases (K25-65459), the US National Cancer Institute (P30 CA034196), the US National Science Foundation (CHE-0722759 and EPS-0132384), the W.M. Keck Foundation, and start-up funds from The Jackson Laboratory and the University of Maine.

#### COMPETING INTERESTS STATEMENT

The authors declare competing financial interests: details accompany the full-text HTML version of the paper at <http://www.nature.com/naturemethods/>.

Published online at <http://www.nature.com/naturemethods/>  
Reprints and permissions information is available online at <http://npg.nature.com/reprintsandpermissions>

- Hell, S.W. *Science* **316**, 1153–1158 (2007).
- Hess, S.T., Girirajan, T.P.K. & Mason, M.D. *Biophys. J.* **91**, 4258–4272 (2006).
- Betzig, E. *et al. Science* **313**, 1642–1645 (2006).
- Rust, M.J., Bates, M. & Zhuang, X. *Nat. Methods* **3**, 793–795 (2006).
- Bock, H. *et al. Appl. Phys. B* **88**, 161–165 (2007).
- Foellmer, J. *et al. Angew. Chem. Int. Ed.* **46**, 6266–6270 (2007).
- Toprak, E. & Selvin, P.R. *Annu. Rev. Biophys. Biomol. Struct.* **36**, 349–369 (2007).
- Bewersdorf, J., Bennett, B.T. & Knight, K.L. *Proc. Natl. Acad. Sci. USA* **103**, 18137–18142 (2006).
- Willig, K.I., Harke, B., Medda, R. & Hell, S.W. *Nat. Methods* **4**, 915–918 (2007).
- Huang, B., Wang, W., Bates, M. & Zhuang, X. *Science* **319**, 810–813 (2008).
- Prabhat, P., Ram, S., Ward, E.S. & Ober, R.J. *IEEE Trans. Nanobioscience* **3**, 237–242 (2004).
- Toprak, E., Balci, H., Blehm, B.H. & Selvin, P.R. *Nano Lett.* **7**, 2043–2045 (2007).
- Prabhat, P. *et al. Proc. Natl. Acad. Sci. USA* **104**, 5889–5894 (2007).
- Hess, S.T. *et al. Proc. Natl. Acad. Sci. USA* **104**, 17370–17375 (2007).
- Schneider, M., Barozzi, S., Testa, I., Faretta, M. & Diaspro, A. *Biophys. J.* **89**, 1346–1352 (2005).